Sensitivity of the Continental Hydrological Cycle to the Spatial Resolution over the Iberian Peninsula

S. VÉRANT

Laboratoire de Météorologie Dynamique, Université Pierre et Marie Curie, and Ecole Nationale du Génie Rural, des Eaux et des Forêts, Paris, France

K. LAVAL AND J. POLCHER

Laboratoire de Météorologie Dynamique, Université Pierre et Marie Curie, Paris, France

M. DE CASTRO

Facultad de Ciencias del Medio Ambiente, Toledo, Spain

(Manuscript received 5 December 2002, in final form 18 July 2003)

ABSTRACT

In the broad context of the downscaling methods that are used to study climatic change impacts, the dependence of the surface hydrological processes simulated by the Organising Carbon and Hydrology in Dynamic Ecosystem (ORCHIDEE) land surface model, used in a stand-alone mode, on the spatial scale of the forcings is investigated over the Iberian Peninsula. These prescribed forcings are the outputs of a regional climate model, Pronóstico a Mesoescala (PROMES), with a high spatial resolution (20 km). In the first experiment, the PROMES outputs have been aggregated stepwise to the typical resolution of a general circulation model, and applied to ORCHIDEE, in order to analyze the impacts of the changing resolution on the simulated water balance. Then, subgrid-scale variability (SSV) for the different forcings has been progressively reintroduced. This second experiment is aimed at isolating the crucial elements of SSV that need to be preserved when a disaggregation is being performed.

The increase of interception loss when the spatial resolution goes beyond 100 km leads to unrealistic values of the interception loss ratio. In the northern humid region, the reduction of runoff frequency when the forcings are aggregated explains the decrease in runoff production, which can reach half the high-resolution runoff. These impacts drive the adjustment of the other hydrological components. The large increase of interception loss is compensated by a reduced transpiration in a dry climate, which induces a large change in soil moisture content, and by reduced runoff in humid regions. The second experiment underlines the dominant effect of precipitation SSV, and particularly the rainfall frequency, on the correct simulation of the water balance. The significant influence of the thermodynamic variables is also analyzed.

1. Introduction

The most commonly used method for predicting future changes in climate is the use of general circulation models (GCMs). They are usually coupled to a land surface model (LSM) that is at the interface between the atmosphere and the soil–vegetation system and closes the water and energy balances. Such models provide scenarios of the evolution of climate at coarse resolution. Yet, at the GCM scale, many subgrid-scale processes are unresolved. The surface—soil texture, vegetation, altitude—is strongly heterogeneous and these contrasts influence the different hydrologic and energetic processes. In addition, atmospheric variables like precipitation have large subgrid-scale variability at the synoptic scale and underlying processes are unresolved at that scale.

Different downscaling techniques aim at relating local-scale climate variables to the large-scale atmospheric forcings. They are employed to try to infer the correct local impacts of climate change from the coarse-resolution scenarios provided by GCMs (Giorgi and Mearns 1991; Hewitson and Crane 1996; Mearns et al. 1999). The two main categories are 1) nested regional climate modeling (Giorgi 1990; Giorgi and Mearns 1999) and 2) semi-empirical statistical downscaling methods (Zorita and von Storch 1999).

The following study takes place in this broad context of downscaling GCM outputs to infer local impacts of climate change. We put the emphasis on a particular region, the Iberian Peninsula, which adjoins the Med-

Corresponding author address: Sylvie Vérant, LMD, Université Pierre et Marie Curie, 4, Place Jussieu, B.P. 99, 75252 Paris Cedex 5, France.
E-mail: sverant@lmd.jussieu.fr

iterranean area. This area is climatically stressed by limited water resources, and over the past centuries, extended dry periods have occurred. Consequently, the possible consequences of climate change on water resources is important to the Iberian Peninsula (Bolle 2003). The new integrated LSM of the Institut Pierre-Simon Laplace (IPSL), the Organising Carbon and Hydrology in Dynamic Ecosystems (ORCHIDEE) model, is used in a stand-alone mode, which is to say with prescribed radiative and atmospheric forcings, to simulate hydrological processes and more precisely quantities such as latent heat flux, runoff, and soil wetness over the Iberian Peninsula. The prescribed forcings are the outputs of a regional climate model (RCM) over the Iberian Peninsula, Pronóstico a Mesoescala (PROMES) (Arribas et al. 2003), forced at its boundaries by data from the European Centre for Medium-Range Weather Forecasts (ECMWF), at a resolution of 20 km $\times$ 20 km (which is a much higher spatial resolution than a typical GCM) during 1 yr (from March 1993 to February 1994). Thus, the starting point of this study consists of high spatial and temporal resolution precipitation, thermodynamic conditions, and land surface properties that are considered to be an approximate ''reality'' at the resolution of 20 km $\times$ 20 km. From these high-resolution RCM outputs, we rebuild the GCM low-resolution forcings by averaging. The main purpose is to identify the crucial variables for which subgrid-scale variability is needed to simulate a satisfactory regional water budget over the Iberian Peninsula.

As a first step, we have previously tried to evaluate how the water budget at regional scale is impacted by a varying subgrid-scale variability of the atmospheric and surface processes. For this purpose, the high subgrid-scale variability of the RCM outputs has been progressively reduced by spatial averaging of the forcings. We then focused on our main objective by reintroducing subgrid-scale variability for the rain and other forcings progressively.

These objectives are related to the dependence of surface hydrological processes on the spatial scale of the forcings. This issue of the impacts of the forcings aggregation on the simulated surface hydrological processes has already been studied. Some studies have underlined the sensitivity of runoff and snow productions to the progressive aggregation of the forcings over some American basins using hydrological rainfall–runoff models (Koren et al. 1999) or a land surface model (Haddeland et al. 2002) and high-resolution data progressively aggregated. In the frame of the Rhone Aggregation Land Surface Scheme Intercomparison Project (RhoneAGG; Boone et al. 2003), the influence of the progressive aggregation of the forcings on the evapotranspiration, runoff, and snow amounts simulated by various land surface schemes has been analyzed. Other stand-alone simulations have compared regional results obtained with high-resolution forcings or with averaged data and have emphasized the hydrological sensitivity to the spatial resolution (Arola and Lettenmaier 1996; Ghan et al. 1997). From another point of view, the significant impacts on the hydrological budget of the subgrid-scale variabilities of precipitation intensity and frequency are well documented. Various stand-alone simulations have already noted the modification of the partitioning between runoff and evaporation when the precipitation coverage is modified (Pitman et al. 1990; Seth et al. 1994; Liang et al. 1996).

It has also been pointed out that the lack of feedback between the land surface and the atmosphere in a stand-alone simulation may in fact modify the sensibility of the surface processes to the spatial resolution of the forcings (Pitman et al. 1993; Dolman and Gregory 1992). For example, an increase of cloud coverage due to moister and cooler air could modify the incoming solar radiation (Wang and Eltahir 2000). In the case of a coupled simulation, if the resolution of the atmospheric forcings is modified, the effects of the spatial resolution on the simulated climate and on the surface water balance are mixed and it is difficult to isolate one from another.

Our experiment allows us to isolate the effects of the aggregation of the forcings on the surface water balance over the Iberian Peninsula and to infer which variables and which properties of these variables need to be reconstructed when a disaggregation is carried out. Section 2 describes briefly the model used in this study and the experiments performed. The model is validated in section 3. Results from the experiments and their interpretation are presented in sections 4 and 5, at regional and local scales. Section 4 emphasizes the effects on the land surface water cycle of the aggregation of the forcings and section 5 deals with the disaggregation of the forcings. Finally, section 6 is a summary of the different conclusions of the study.

2. Model description and experimental design

a. Brief description of ORCHIDEE

ORCHIDEE is the new LSM of the IPSL. It has been developed for regional studies either within a GCM or in a stand-alone mode. It is composed of 1) the previous LSM of the Laboratoire de Météorologie Dynamique, Schématisation des Echanges Hydriques à l'Interface entre la Biosphère et l'Atmosphère (SECHIBA), which computes the physical processes at the interface between soil, vegetation, and atmosphere and the water fluxes in the soil (Ducoudré et al. 1993); 2) the carbon cycle model of the Laboratoire des Sciences du Climat et de l'Environnement, Saclay Toulouse Orsay Model for the Analysis of Terrestrial Ecosystems (STOMATE), which simulates the biochemical processes at the surface (Viovy 1996), 3) the Lund–Potsdam–Jena (LPJ) model, which represents the dynamical evolution of the vegetation and the carbon budget (Sitch et al. 2000). The

TABLE 1. The aggregation experiment: horizontal resolution (km) of the forcings (*P*, precipitation; *R*, radiation; *W*, wind; *T*, air temperature; *Q*, air humidity; and P_s, surface pressure) and of the land surface (km) for each performed simulation.

	Resolution (km)						
	Forcing						Land surface resolution
Simulation	*P*	*R*	*W*	*T*	*Q*	P_s	
Group 1							
Agg20	20	20	20	20	20	20	20
Agg40	40	40	40	40	40	40	40
—							
Agg240	240	240	240	240	240	240	240

TABLE 2. The ''disaggregation'' experiment: horizontal resolution (km) of the forcings (*P*, precipitation; *R*, radiation; *W*, wind; *T*, air temperature; *Q*, air humidity; and P_s, surface pressure) and of the land surface (km) for each simulation.

	Resolution (km)						
	Forcing						Land surface resolution
Simulation	*P*	*R*	*W*	*T*	*Q*	P_s	
Group 2							
Mean	240	240	240	240	240	240	20
P_{freq}-mean	20*	240	240	240	240	240	20
P-mean	20	240	240	240	240	240	20
PR-mean	20	20	240	240	240	240	20
PRW-mean	20	20	20	240	240	240	20
PTQ-mean	20	240	240	20	20	240	20
PTQPs-mean	20	240	240	20	20	20	20

two last components of ORCHIDEE are not used in this study.

The vegetation distribution in ORCHIDEE is based on the International Geosphere–Biosphere Programme (IGBP) land cover map. It is described in appendix A. The soil hydrology consists of two moisture layers with the upper one having varying depth. The total soil depth is constant at 2 and the soil has a maximum water content per unit of soil volume (150 kg m^{-3}) (Ducoudré et al. 1993). Runoff occurs when the soil is saturated (Dunne's saturation excess concept of runoff generation) and it is the only runoff mechanism in the model. The routing scheme implemented in the model is presented in appendix B.

Another mechanism for inducing surface runoff, occuring when the precipitation rate is higher than the infiltration rate, and called Horton runoff (Entekhabi and Eagleson 1989), is not taken into account in this model whereas it could be an important process, for example, in semiarid areas (Liang and Xie 2001). In addition, runoff is usually controlled by spatial heterogeneity in precipitation and surface conditions like topography or soil moisture. These heterogeneities are also not taken into account in the model. It is thus clear that our runoff formulation is crude (Koster et al. 2000; Warrach et al. 2002). Consequently, the simulated runoff may possibly have some biases.

The control of evapotranspiration by the soil–plant system is presented in appendix C and described more fully by de Rosnay and Polcher (1998).

b. Experimental design

The aggregation method employed to increase the size of the grid boxes from 20 km × 20 km to (20*n*) km × (20*n*) km ($n = 2, 3, 4, \ldots$) and thus to generate a pseudo-GCM forcing is very simple. For each variable and at each time step, the 20 km × 20 km cells are gathered n^2 by n^2 and the mean of the n^2 values is allocated as new value to a (20*n*) km × (20*n*) km cell. A reference forcing file with high-resolution variables (PROMES output) and different mean forcing files with spatially aggregated variables up to 240 km × 240 km ($n = 12$) are then constructed in order to force ORCHIDEE. Simultaneously, the land surface properties can either be aggregated up to the new resolution of the forcings or held constant at a resolution of 20 km × 20 km. The ''disaggregation'' method is also elementary, but perfect for our objective. In order to reintroduce subgrid-scale variability, high-resolution variables from the original forcing file (RCM outputs) are used to modify the mean 240 km × 240 km forcing file. In this study, the purpose is to evaluate which input variables must retain their subgrid-scale variability in the forcings to simulate a correct water balance. The simplest method is used to introduce subgrid-scale variability since the ''true'' high-resolution forcings, the high-resolution variables from the original forcing file, are used.

With each forcing file used as climatological input, a 5-yr simulation of the continental water cycle is performed by ORCHIDEE. The time step of each forcing file is 3 h. It is interpolated to a 30-min time step for the simulation. The duration of the simulation (5 yr) is needed to bring the water cycle to an equilibrium. Only the last year of the simulation will be studied.

The reference simulation is performed with high-resolution forcings and high-resolution vegetation. It will be referred to as simulation Agg20.

In the first group of simulations (cf. Table 1), the forcings and the land surface (i.e., principally the vegetation distribution) have the same resolution. Simulations with horizontal resolutions of 20, 40, 60, 80, 120, and 240 km are performed. Each of these simulations will be referred to as the simulation Agg*m* where *m* is the horizontal resolution in kilometers ($m = 20, 40, \ldots, 240$).

In a second group of simulations (cf. Table 2), the land surface resolution is kept at 20 km × 20 km. Consequently, all of the simulations are performed at this resolution. When a forcing variable is averaged at 240-km resolution, the same averaged value is applied to each of the 20 km × 20 km cells contained in the coarser grid box. All of the forcings are averaged at 240-km resolution in the simulation Mean. Consequently, the only difference between this last simulation (Mean) and the simulation Agg240 is the land surface resolution.

The variables precipitation (P), radiation (R), wind (W), air temperature (T), and humidity (Q) and surface pressure (P_s) are then ''disaggregated'' one after another. The performed simulations will be referred to as simulations xxx-mean, where xxx stands for the abbreviations of the disaggregated variables, with all other variables being averaged at 240-km resolution. For example, in the simulation named PR-mean, only the precipitation and radiation are disaggregated.

In the simulation P_{freq}-mean, the only variable that is partly kept at high resolution is the precipitation. All the other variables are averaged at 240-km resolution. More precisely, in this simulation, the true spatial distribution of precipitation occurrence is preserved but the precipitation amount allocated to each small cell is the precipitation average over the grid boxes within the large grid box where precipitation occurs.

3. Validation of the reference simulation

The purpose of this section is to establish the confidence in the validity of the model ORCHIDEE by showing that it produces simulations of the hydrological cycle over the Iberian Peninsula in agreement with observations for the studied year (from March 1993 to February 1994). Two major components of the hydrological cycle are compared with observations: the precipitation field and the river discharges to the ocean. The precipitation field is a crucial input for the correct simulation of the water cycle by ORCHIDEE. It is simulated by the RCM PROMES at high spatial resolution. It will be compared to areal Climate Research Unit (CRU) observations at $0.5° \times 0.5°$ resolution (New et al. 2000) and to point time series at the various stations provided by the European Climate Assessment (ECA) project (Tank et al. 2002) for the corresponding year. The discharges to the ocean of the main rivers of the Iberian Penisula are integrated outputs simulated by the land surface scheme. They will be compared to interannual averages of the Global Runoff Data Center (GRDC) river discharges.

The validation of regional high-resolution simulations relies on the available observations. For precipitation, point time series and areal global fields are available. The resolution of the areal observations depends on the density of the observing network, which is interpolated to build the areal dataset. In the present case, the resolution of CRU is coarser than the RCM resolution. The PROMES outputs will be smoothed to be compared to the CRU observations. Some local information may be lost and cannot be evaluated through this comparison.

In order to validate high-resolution variability, point observations may be used. Yet, point observations are not fully representative of an average grid box due to the subgrid-scale variability of land surface properties and atmospheric conditions. Ignoring this potential error, point precipitation time series will be compared to the model value at the grid point closest to the observation.

a. Comparison to CRU areal precipitation

The spatial resolution of the PROMES fields is higher than the resolution of the CRU datasets. The PROMES outputs must be interpolated to match the observation resolution. They are interpolated to a regular $0.5° \times 0.5°$ grid corresponding to the CRU grid. The comparison is limited to the winter and summer seasons (cf. Fig. 1).

In winter, moist air advection or midlatitude cyclones generated over the Atlantic Ocean and reaching the Iberian Peninsula are able to produce precipitation over northwestern and northern areas. This process is related to large-scale circulation and seems realistically reproduced by the simulation, which shows good agreement of the precipitation field between the model and the observations. Let us point out that PROMES is forced at its boundaries by ECMWF large-scale fields, and this can partly explain these good results. Yet, the spatial variability is higher in the PROMES case and the local dry–wet contrasts are more numerous compared to the smooth spatial variations of the CRU values. This does not mean that this simulated variability is unrealistic. We show in a comparison of the model results for data from a station (Porto) located at the limits of this humid area that PROMES simulates a type of precipitation that reproduces the observations very well. Another area of agreement between the observations and the model results is the NW–SE-oriented gradient over the region that is also rather well represented although the dry area is more spread out in the southeastern part of the peninsula in the model.

In summer, the contrast between the humid northern region and dry southern one is also correctly reproduced. The simulated field shows an incursion of higher precipitation southward (near 41.5°N) that does not occur in the interpolated dataset. The precipitation maxima over the mountaineous regions like the Pyrenees are stronger in PROMES than in CRU. These differences may be related to the fact that precipitation is strongly related to orography in the PROMES model (Gaertner et al. 2001).

Overall, the model and the observed precipitation show many similar features.

b. Comparison to ECA point time series

CRU precipitation fields are spatial averages at relatively low resolution compared to PROMES fields. Point measured time series are compared to PROMES values at the nearest grid point in order to reinforce our confidence in the high-resolution variability of PROMES.

Table 3 presents a comparison between observed and model annual precipitation at 16 stations distributed

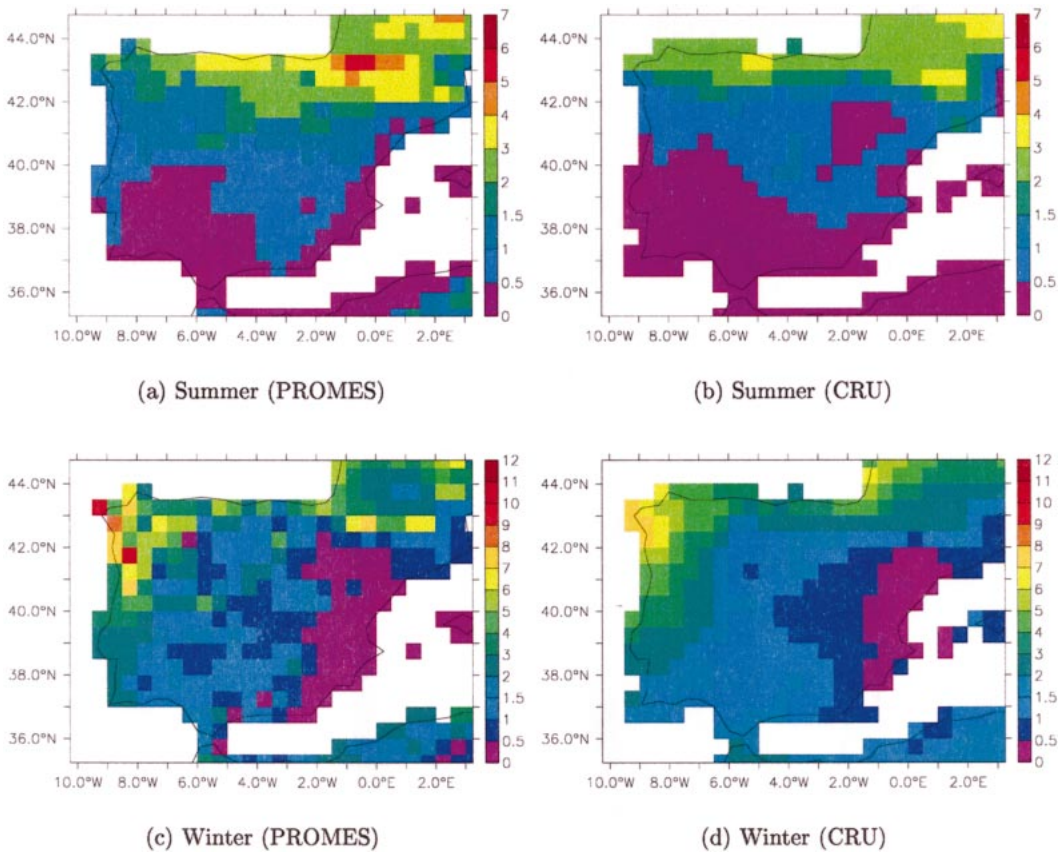

FIG. 1. Seasonal precipitation amounts (mm day^{-1}) simulated by the model (PROMES) in (a) summer and (c) winter and observed (CRU) in (b) summer and (d) winter.

over the Iberian Peninsula for the year 1993–94 (cf. Fig. 2). The results on an annual scale are better for the western part of the peninsula than for the interior of the peninsula and for the eastern coast. This suggests that the model is less successful in reproducing the mesoscale systems that can produce isolated convective events or recycling of evaporated water. It also shows that semiarid zones are more difficult to simulate with these models.

Figure 3 presents a comparison of monthly results for 4 stations among the 16: we choose 2 of them over humid areas and 2 over dry areas (the least successful) where the total annual precipitation was 40% off ob-

TABLE 3. Annual precipitation amount (mm yr^{-1}) [the deviation from the observations (in %) is indicated in parentheses].

Station name	PROMES	ECA
Badajoz	279 (−31)	471
Beja	521 (−18)	632
Braganca	909 (−6)	970
Coimbra	988 (−23)	1276
Lisbon	635 (−24)	839
Madrid	468 (−4)	487
Malaga	332 (−33)	499
Navacerrada	829 (−33)	1236
Porto	1349 (−11)	1517
Salamanca	402 (−14)	469
San Sebastian	1753 (+7)	1636
Tavira	546 (+8)	504
Torrevieja	132 (+16)	152
Tortosa	240 (−44)	430
Valencia	182 (−38)	294
Zaragoza	431 (+57)	275

FIG. 2. Localization of the ECA stations.

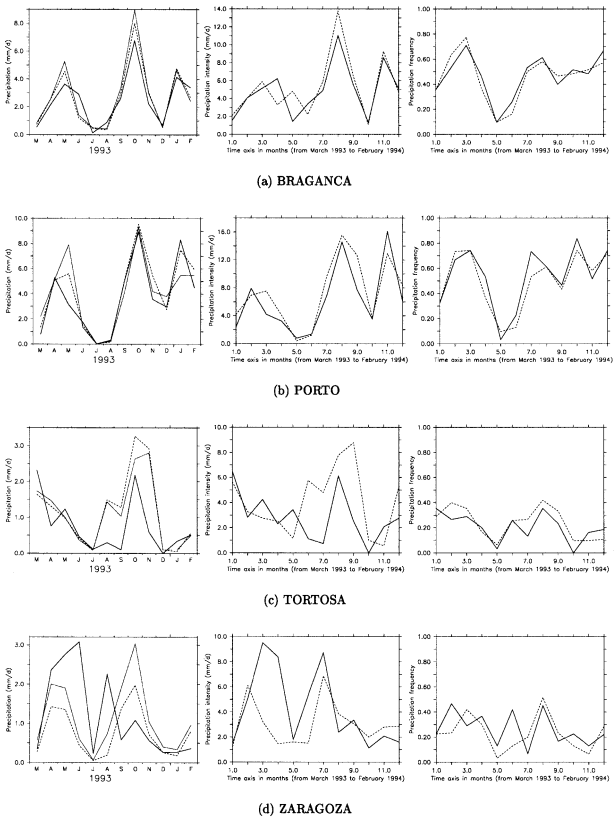

FIG. 3. (left) Comparison of monthly precipitation (mm day^{-1}), (middle) precipitation intensity (mm day^{-1} of precipitation), and (right) frequency between model simulation (solid line), ECA (dashed lines), and CRU (dotted lines) observations, for the stations (a) Braganca, (b) Porto, (c) Tortosa, and (d) Zaragoza.

served. The Braganca and Porto precipitation time series are reproduced remarkably well by the model. Precipitation is the combination of an occurence process and of intensity. Both processes are correctly simulated. On the contrary, as expected, the results are poor for Zaragoza and Tortosa. The precipitation is largely underestimated in autumn for Tortosa. The precipitation intensity is much lower than it should be. In the case of Zaragoza, the three maxima in the PROMES outputs correspond to two maxima in the data, which means the annual cycle is not properly represented. The seasonal precipitation amounts are largely overestimated in spring and summer. However, for these two stations, the frequency of the precipitation is not as poorly represented and it seems that the model is quite unrealistic in precipitation intensity.

c. Comparison to GRDC discharge

In this section, we compare an integrated variable of the hydrological cycle, the river discharge. It is calculated directly by the land surface scheme (briefly described in appendix B). For different major rivers of the Iberian Peninsula (Ebro, Douro, Tejo, Guadalquivir; cf. Fig. 4), the model riverflows are compared to interannual averages and standard deviations of GRDC river discharges (cf. Fig. 5) as data for 1993–94 are not available and the routing scheme could not be initialized for the previous years.

Figure 5 compares river discharges simulated by the model to GRDC interannual averages and monthly precipitation over the basin area to CRU observations. The Douro and Tejo precipitation totals are well reproduced even if the spring (and autumn for the Douro) maxima are underestimated. Over the Ebro basin the precipitation amounts are overestimated in summer and underestimated in autumn when compared to CRU, and for the Guadalquivir basin, the autumn and winter precipitation amounts are underestimated. These deficiencies of the precipitation simulation must be kept in mind for the river discharge comparison.

For the Ebro, Douro, and Tejo, the annual discharge cycle remains within the interval of interannual variability. The annual cycle is well represented even if during the low-flow period (August–September) the discharges are slightly underestimated. In the southern region (Guadalquivir), the simulation is not satisfactory. The annual amount is largely underestimated and the low-flow period is not properly simulated. The underestimated precipitation may explain part of this deficiency but the runoff generation mechanism, which is not adapted to this semiarid region, probably has the most significant influence.

In addition, the irrigation is not simulated by the model whereas it must have significant impacts on the Guadalquivir discharge in particular since irrigation is highly developed in southern Spain.

For the moment, the model ORCHIDEE takes into account neither the dams nor the irrigation outputs/inputs to the soil reservoirs. The induced modifications of the natural riverflows must be significant and so to must be the errors we make when comparing our results to these data. Nevertheless, the discharges produced by the model over the Iberian Peninsula are in general agreement with observations.

4. Aggregation of the climate forcing

The purpose of this section, is to underline the main hydrological effects over the Iberian Peninsula of the progressive aggregation of the forcings. The induced modifications of the interception loss and of the total runoff appear to be the main processes that drive the water balance changes. The transpiration and the soil water content then adjust themselves to the new water input, depending on the climate.

Let us point out that interception is a term that covers an ensemble of processes that result from the temporary storage of precipitation by vegetation. In the model, the processes related to interception are throughfall and interception loss. Throughfall represents the fraction of precipitation that is not intercepted by the canopy and

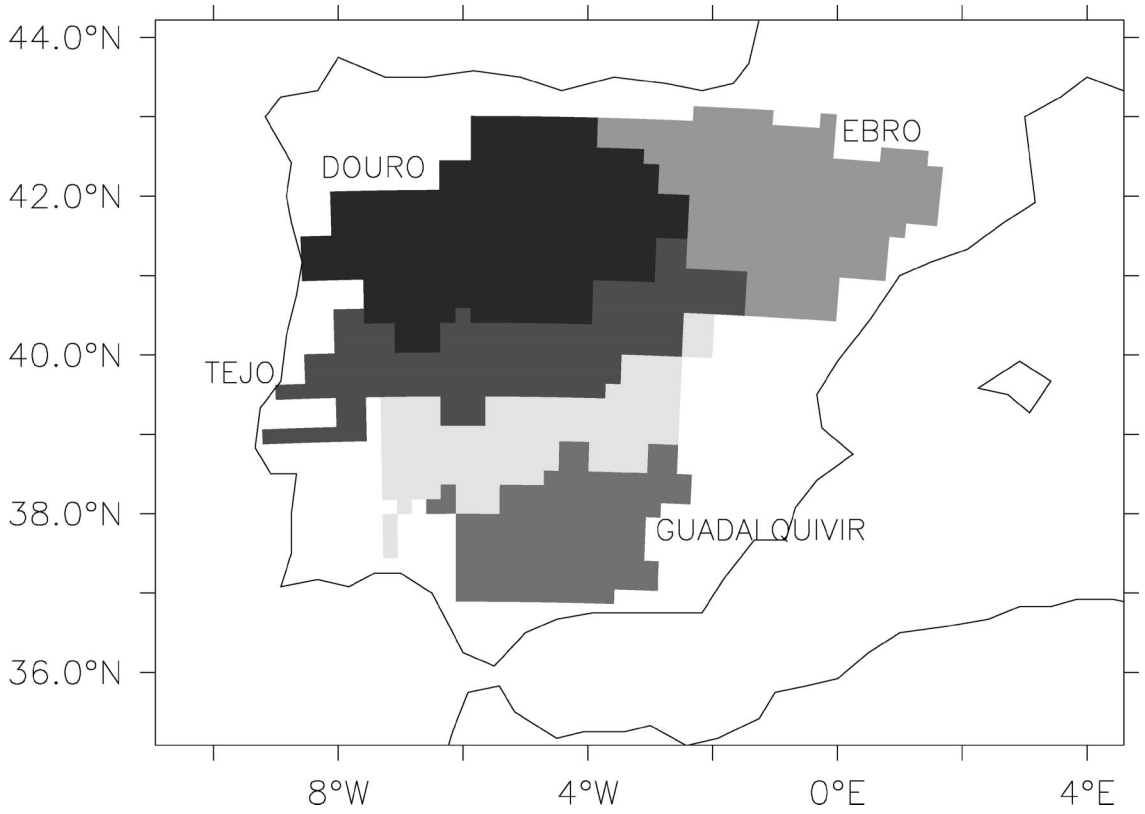

FIG. 4. Approximate map of the major river basins. The lightest gray shading represents an unused river basin, Guadiana.

interception loss accounts for evaporation of the precipitation retained by plant surfaces.

The results are analyzed at 240 km × 240 km resolution, which is the regional scale. In the experiment, the Iberian Peninsula consists of nine regions (or large cells). Among these nine regions, four are described as humid and five as dry. The limit between these two groups of cells (somewhat arbitrary) corresponds to an annual precipitation amount of 500 mm yr^{-1}. For each simulation (Agg40–Agg240), for each region, if the continental area is modified due to the spatial resolution, the point is considered to be missing.

a. Main features of the water cycle simulated by ORCHIDEE

In this section, the main features of the water cycle simulated by ORCHIDEE are presented. Two simulations, Agg20 and Agg240, are compared in two different regions of the Iberian Peninsula: the dry southern part and the humid northern part. Figure 6 presents the annual values of precipitation and both of the chosen regions (among the nine regional cells) are outlined (A is the dry region and B the humid one). These regions are distinguished because the way in which the soil, plants, and the atmosphere interact is different. In this version of the model, runoff only occurs when the soil is saturated. As a consequence, in the dry part of the Iberian Peninsula, since the soil hardly ever reaches the saturation, runoff is negligible. In other studies, the Horton runoff has been taken into account by probability distributed models like the Variable Infiltration Capacity model (VIC; Wood et al. 1992), which introduced a subgrid-scale variability of the infiltration rate. However, the impact of introducting this term in a large-scale model is rather limited (Ducharne et al. 1998) if the grid size of the model is large.

Each simulation performed by ORCHIDEE brings the water cycle to an equilibrium, which implies that precipitation and snowfall input equals the sum of evapotranspiration and runoff at the annual scale. In addition the simulation is performed in a stand-alone mode, without feedback from the land surface to the atmosphere.

Figure 7 presents the mean temporal evolutions of precipitation, transpiration, interception loss, and soil water content in the dry zone (south of the Iberian Peninsula). The absence of rainfall in summer can be noted. In this region, no runoff occurs in the model regardless of what the resolution may be. When the resolution decreases, throughfall is reduced and the interception loss is increased during each rainfall event (cf. Fig. 7c). This point will be developed in the next section. The transpiration adjusts itself to the changed throughfall through the modification of the water content of the soil. It is obtained by a translation of the water content to

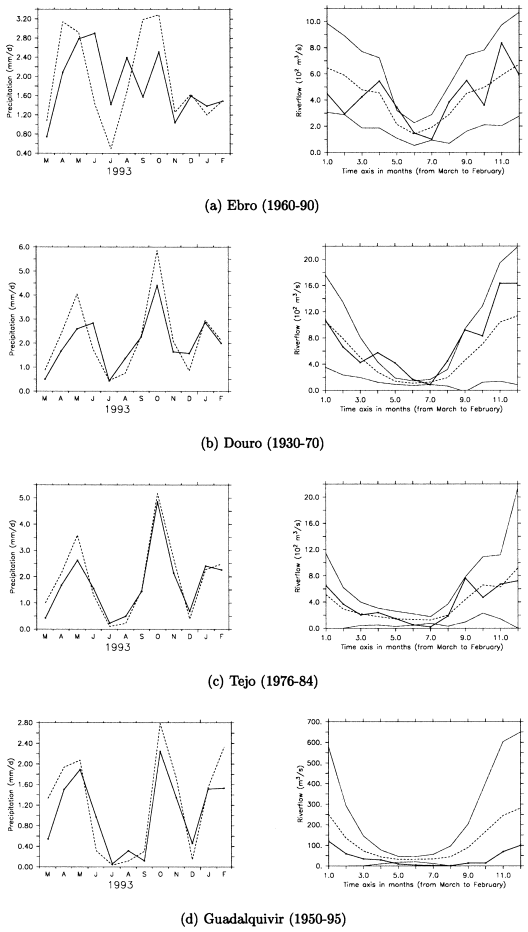

FIG. 5. (left) Monthly precipitation over the basin (mm day^{-1}) and (right) riverflows at the outlet (m^3 s^{-1} or 10^2 m^3 s^{-1}). PROMES precipitation amounts (solid line) are compared to CRU (dashed line) for the year 1993–94; the river discharges (solid line) are compared to an interannual average (dashed line) over a period indicated in parentheses plus or minus one standard deviation (dotted lines): (a) Ebro (1960–90), (b) Douro (1930–70), (c) Tejo (1976–84), and (d) Guadalquivir (1950–95).

lower values (cf. Fig. 7d) and so to an increase of the water stress. Consequently, when the forcings are averaged, the soil water content is smaller throughout the year and the transpiration is reduced (cf. Fig. 7b) mainly in the summer season. This result underlines the importance of subgrid-scale variability in simulating soil moisture content in semiarid regions for GCMs. Our numerical experiment shows that even if the total evapotranspiration has the same rate, the repartition between transpiration and interception loss has a strong impact on soil moisture simulation. In winter, the evaporation flux is limited by the solar radiation. The decrease of the soil humidity has little influence during this season.

Figure 8 presents the mean temporal evolutions of precipitation, runoff, transpiration, interception loss, and soil water content in the humid zone (northern Iberian Peninsula). In this humid region, when the resolution is reduced, interception loss also increases (cf. Fig. 8c) and throughfall is reduced. In fall, the soil water content increase is more spatially regular since the water input is more homogeneous. The combined effects of the reduced throughfall and the more homogeneous water input to the soil explain the delay of about 2 months before runoff begins and the higher spatial mean soil water content in winter in the simulation Agg240. The main governing processes will be detailed in the next section. Transpiration adjusts itself to the increase of interception loss and bare soil evaporation, and to the decrease of runoff but this effect is much smaller than in the dry case. In spring and early summer, the more homogeneous water content allows a slightly stronger transpiration accumulation with coarser resolution. Then, the soil water depletion is increased at the end of summer and early fall. Eventually, in winter, the solar radiation limits the latent heat fluxes and the increased high frequency of precipitation (92% of rainy days compared to 70% in summer) augments the number of days when the foliage is covered with water and the transpiration limited.

The description of the water cycle simulated by ORCHIDEE over the Iberian Peninsula in simulations Agg20 and Agg240 has pointed out the main consequences on the surface fluxes and the soil water content of the spatial aggregation of the forcing. To summarize, in both cases, the resolution increase induces a large decrease of interception loss, which is compensated by transpiration in the dry case and by runoff in humid regions.

b. The impact on interception processes

The interception loss represents 9%–16% of the precipitation in simulation Agg20 over the Iberian Peninsula (cf. Fig. 9). As expected, the interception loss increases when the resolution is coarser. This is explained by reduced spatial variance and increased frequency of the precipitation. Figure 9 also gives some observations of interception loss, which accounts for from less than 5% to more than 35% of the precipitation depending on the location. This ratio depends on the morphology of the canopies in the area and on the dominant precipitation regimes. Over forested sites in the United Kingdom, Calder (1990) reported observations of this ratio that reach 0.35 whereas the measured values in the French Landes vary between 0.1 and 0.16. Over Amazonian forests, presented here as another extreme, the interception loss ratio goes from around 0.09 to 0.18. Measurements of interception loss over low vegetation are much less numerous, as expected (see Fig. 9).

The interception loss ratios that are shown in Fig. 9 are averages over the different 240 km × 240 km grid boxes. Over the Iberian Peninsula, the dominant vegetation types are trees and crops. The low vegetation fractional coverage is higher than 0.45 over most of the peninsula except in the north-western part where trees dominate. Bare soil covers approximately 5%–15% of

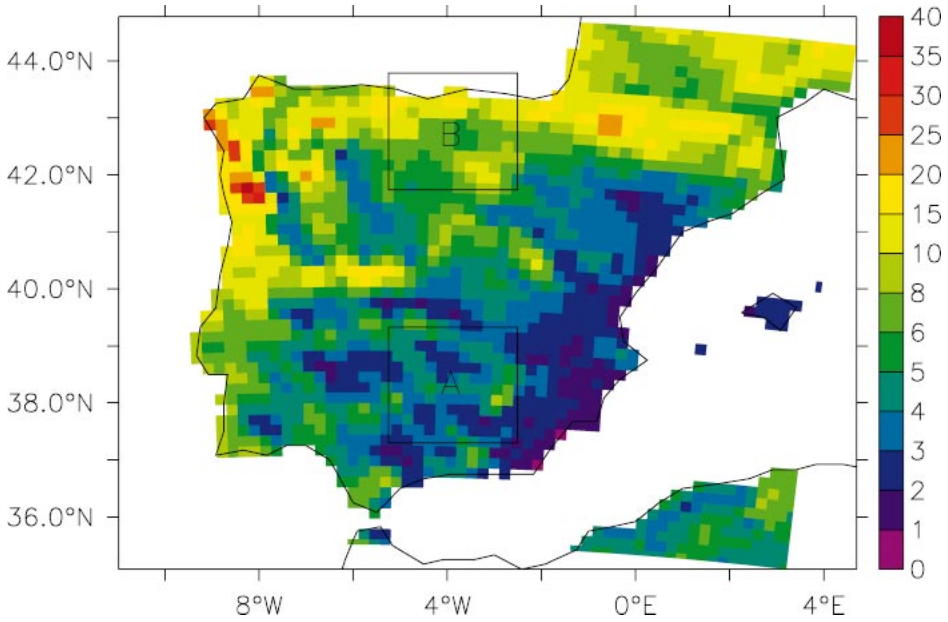

FIG. 6. Annual values of precipitation (10^2 mm yr^{-1}) and outlines of the studied regions (A, dry region; B, humid region).

the surface. The leaf area index reaches a maximum value for trees of 4.5 and 2 for crops but has averaged values over the 240 km × 240 km grid boxes that vary from 1.5 to 3.5. These values are close to the values of 2–3 for the Landes sites and smaller than the estimates of leaf area index from temperate forest sites, which are between 5 and 6 (Scurlock et al. 2001). Thus, the interception loss ratio of 0.1 for the whole wet grid boxes simulated in Agg20 is closer to observations than the result of 0.2–0.3 simulated in Agg240. Over the dry grid boxes, the interception loss ratio is larger than in the humid region, as expected, although the interception loss is lower. The results simulated by Agg20, in the range of 0.13–0.16, seem also much more realistic than the values of 0.3–0.4 obtained with Agg240 in this region where low vegetation covers more than 60% of the surface.

For all grid boxes and for a resolution of lower than 100 km, the simulated interception loss ratio is in the range of 0.2–0.4, which seems quite unrealistic when compared to the different observations.

As a first approximation, the reservoirs in leaves are supposed to be automatically filled up when it rains. This approximation can be justified by considering the sizes of the foliage reservoirs, which are small if compared to the mean daily precipitation. At each time step, when the resolution decreases and when it rains, more reservoirs are supplied with water due to the averaged precipitation. The regional amount of water stored by the foliage is increased as is the interception loss. Figure 10 illustrates the increase of the mean number of rainy days over each region when the spatial resolution is reduced. The limiting value that defines a rainy day (0.2 mm day^{-1}) allows the complete filling of a low vegetation foliage reservoir. This filling is consequently more frequent and the interception loss increases when the resolution gets coarser.

Figure 11 isolates and points out the role of the precipitation resolution in sensitivity since the subgrid-scale variability of the precipitation has a dominant effect on the simulation of the water balance (this point will be illustrated in section 6). This figure is based on three simulations in which only the precipitation distribution is different (Mean, P_{freq}-mean, and P-mean). All of the other variables are averaged at 240 km. A simulation in which the precipitation is averaged at 240 km (Mean) is compared to a simulation in which only the precipitation spatial distribution is reintroduced (P_{freq}-mean) and to a simulation in which the ''true'' precipitation is used (P-mean). Due to the small number of regional cells (nine), no quantitative result can be established. The idea is to place an emphasis on qualitative results. The increase of interception loss between P-mean and Mean goes from approximately 60% to 110% of P-mean for the different 240 km × 240 km cells (cf. Fig. 11). It is composed of an increase of about 30% when the water is uniformely distributed only on the cells where the precipitation is different from 0 (from P-mean to P_{freq}-mean). Between these two simulations, P-mean and P_{freq}-mean, the precipitation spatial distribution is preserved and only its intensity is modified.

Figure 11 illustrates that, over the Iberian Peninsula, the influence of the precipitation intensity, which is not negligible, depends neither on the climate nor on the surface characteristics since the relative difference between P-mean and P_{freq}-mean is constant (30%). The

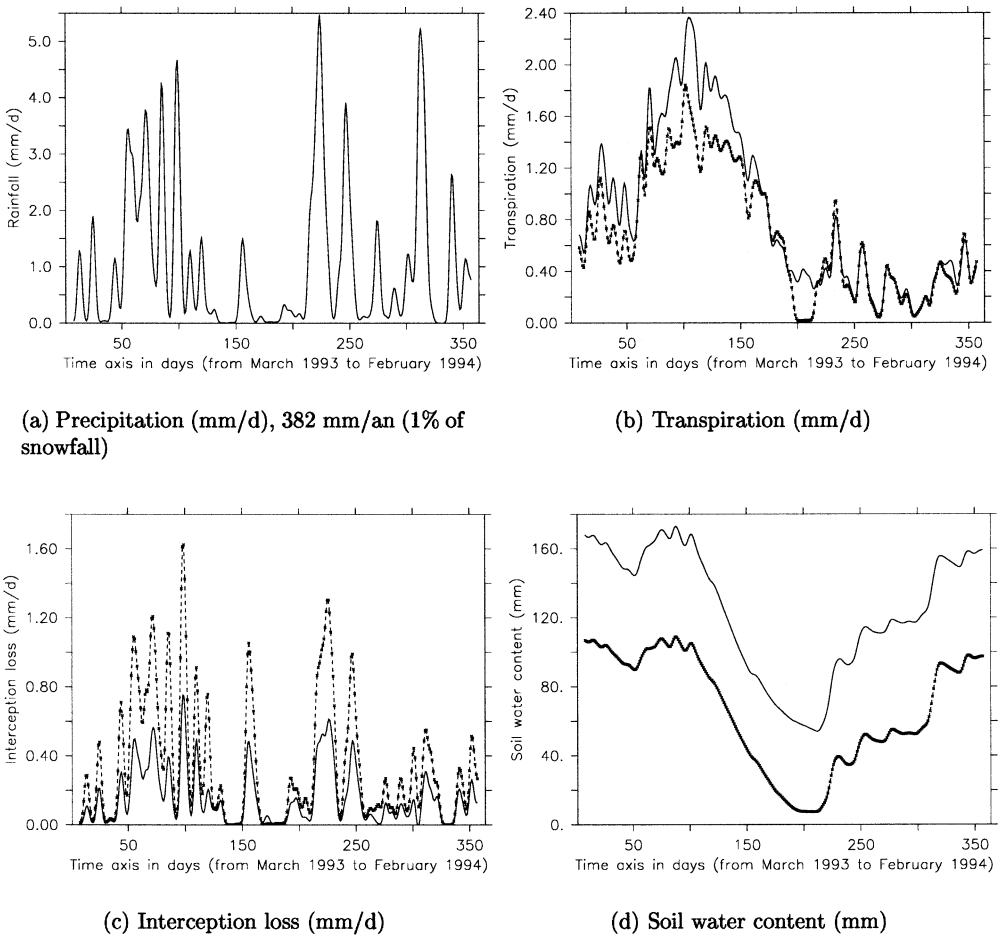

FIG. 7. Annual cycle of the water balance components in the dry region: (a) precipitation (mm day^{-1}), 382 mm yr^{-1} (1% snowfall), (b) tranpiration (mm day^{-1}), (c) interception loss (mm day^{-1}), and (d) soil water content (mm). Solid lines correspond to simulation Agg20, and dashed lines with crosses to simulation Agg240. A binomial window of 15 days was applied to smooth each variable along the temporal axis.

explanation of this influence can be found in the temporal variability of the precipitation daily amount throughout the year. The increase of 30% of a relative interception of 0.15 is not very large although the resolution is changed from 20 km $\times$ 20 km to 240 km $\times$ 240 km. This underlines the fact that interception loss is much less sensitive to precipitation intensity than to precipitation frequency. This result is in agreement with the analysis of Rutter (1975), which shows the larger influence of the precipitation regime than of precipitation intensity. In the numerical experiment analyzed here, the absence of the precipitation spatial distribution (i.e., the difference between P_{freq}-mean and Mean) is generally responsible for more than half of the interception loss increase. The spread of the response is much larger for this second effect and should be linked to the total volume of the foliage reservoirs that do not receive water. This volume is correlated to the increase of the interception loss. The larger this volume (which does not receive water in the simulation P_{freq}-mean), the larger the increase of the interception loss between P_{freq}-mean and Mean. Yet, this correlation is modulated by the precipitation distribution during the year (not shown).

The season has a small impact on the increase of the interception loss. The interception loss depends on the precipitation amount (water input) and also on the solar radiation (energy input). These two limiting factors interact. The solar radiation limits the interception loss in winter, and the small summer precipitation over some cells can limit the summertime interception loss whereas the evaporative demand is stronger in this season. Due to stronger evaporative demand, the interception loss is more important in summer than in winter provided there is enough precipitation. When the spatial resolution of the forcings is reduced, the increase of the interception loss is more important in summer than in winter (not shown). This can be explained by the stronger evaporative demand. This, also, is illustrated in Rutter's analysis (his Fig. 4).

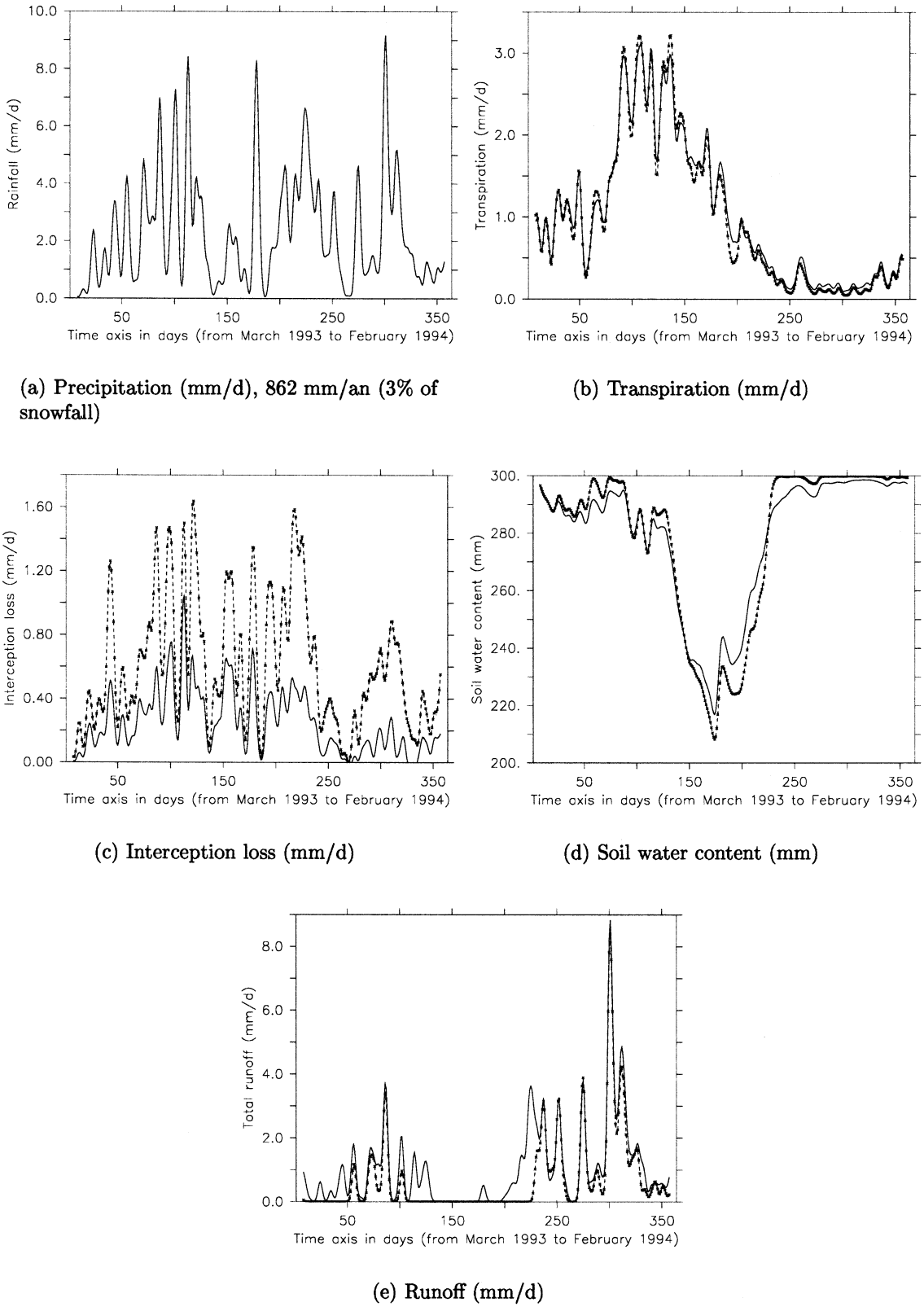

FIG. 8. Annual cycle of the water balance components in the humid region: (a) precipitation (mm day^{-1}), 862 mm yr (3% snowfall), (b) tranpiration (mm day^{-1}), (c) interception loss (mm day^{-1}), (d) soil water content (mm), and (e) runoff (mm day^{-1}). Solid lines correspond to simulation Agg20, and dashed lines with crosses to simulation Agg240. A binomial window of 15 days was applied to smooth each variable along the temporal axis.

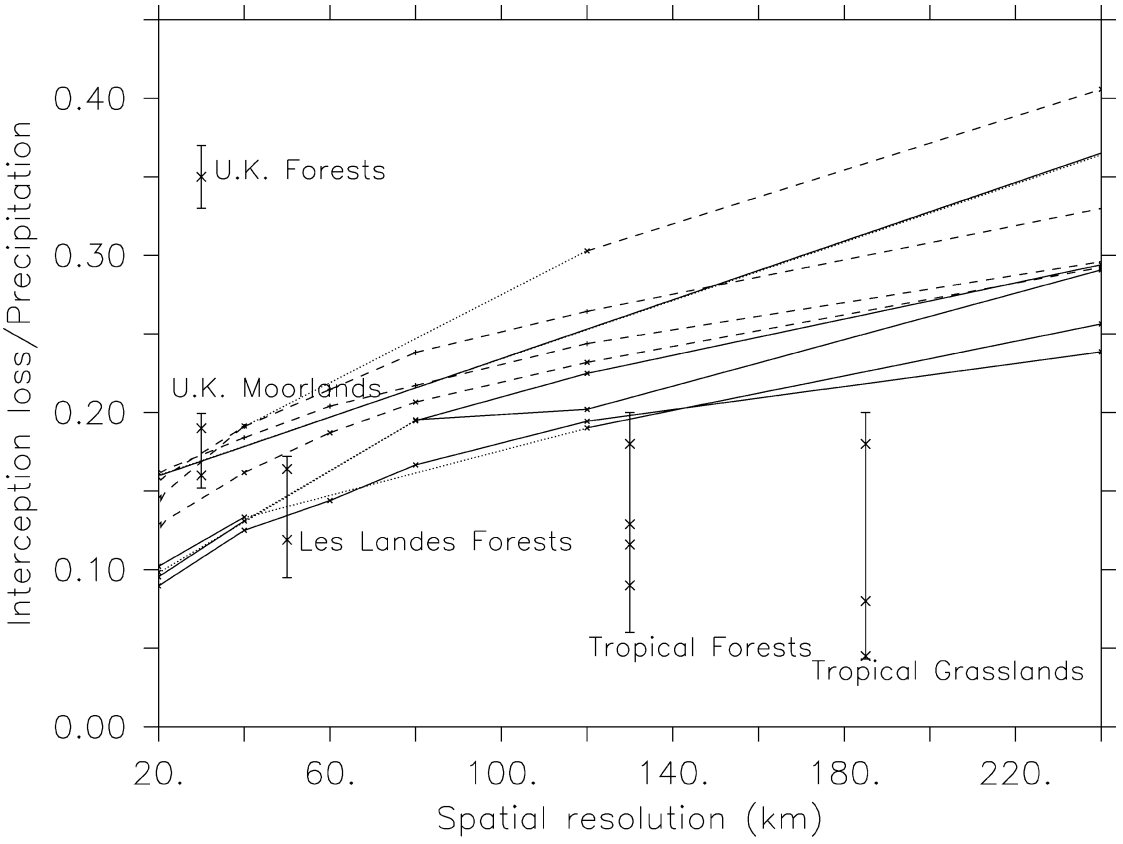

FIG. 9. Increase of the annual mean interception part in the total precipitation with the resolution (simulations Agg20, Agg40, Agg60, Agg80, Agg120, and Agg240 are compared at 240 km). Solid (dashed) lines correspond to humid (dry) grid boxes (dotted lines link points between which values are missing). Vertical bars correspond to measured values (xs) of interception loss ratios with estimated errors intervals over different gathered sites (the horizontal location of the bars does not correspond to any spatial resolution): various temperate forests in Wales and Scotland (for annual rainfall regime exceeding 1000 mm) (Calder 1990); two moorlands in England (Calder 1990); two maritime pine forests in Les Landes from the Hapex-Mobilhy experiment (1 yr) (Gash et al. 1995), and from another site near Bordeaux (2 yr) (Loustau et al. 1992); a tropical forest at Reserva Duck, near Manaus (2-yr period) (Lloyd and Marques 1988); two tropical forests—Reserva Jaru and Reserva Vale do Rio Doce—from the Abracos project (for an entire period of 15 months of observations) (Ubarana 1996); a tropical pine plantation on former grassland soil (1 yr) (Waterloo et al. 1999); and a tropical upland mixed cropping system (around 6 months) (van Dijk and Bruijnzeel 2001).

c. The impact on runoff

The decrease of the model resolution is also expected to play an important role in the runoff simulation. Different studies have shown that runoff generation decreases as the resolution gets coarser (Milly and Eagleson 1988; Seth et al. 1994; Ghan et al. 1997; Koren et al. 1999; Boone et al. 2003). Our study is qualitatively consistent with these results as shown in Fig. 12a.

Only the behavior of the moister part of the Iberian Peninsula is presented. When the forcings are aggregated, 1) the number of days of runoff is reduced and 2) runoff intensity is increased (cf. Figs. 12b and 12c). Throughfall is reduced and the water input to the soil is more homogeneous over the grid boxes. Consequently, runoff starts later and ends earlier (cf. Fig. 8c). This explains the reduction in the number of runoff days. However, more cells are saturated at the same time since the water is uniformely distributed, which explains the increase in runoff intensity. These two consequences of the aggregation of the forcing have opposite influences. Yet, runoff amount is reduced. The reduction in the number of days of runoff has a dominant effect.

Runoff is mainly reduced in the fall while the soil is being filled with water. Between simulations Agg20 and Agg240, the runoff in the fall decreases by 40%–95% (cf. Fig. 13a). In winter, more than 80% of the runoff amount is preserved (cf. Fig. 13b). During this period, the soil is saturated and the evaporation is strongly limited by the low solar radiation. Overall, over the moister part of the Iberian Peninsula, the runoff decreases by 35%–55% between Agg20 and Agg240. It is clearly shown that Agg240 simulates strongly biased values, and the necessity of computing runoff at high resolution is emphasized by these results.

The impact of the aggregation of the forcing on the runoff production is largely constrained by the runoff-

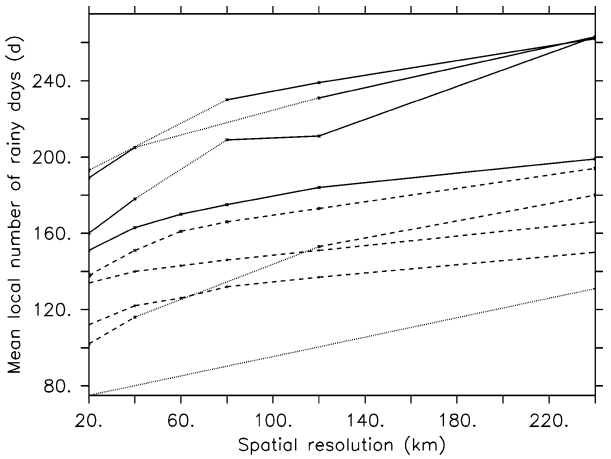

FIG. 10. Increase of the mean local annual number of rainy days (the threshold defining a rainy day is 0.2 mm day^{-1}) with spatial resolution (simulations Agg20, Agg40, Agg60, Agg80, Agg120, and Agg240 are compared at 240 km). Solid (dashed) lines correspond to humid (dry) grid boxes (dotted lines link points between which values are missing).

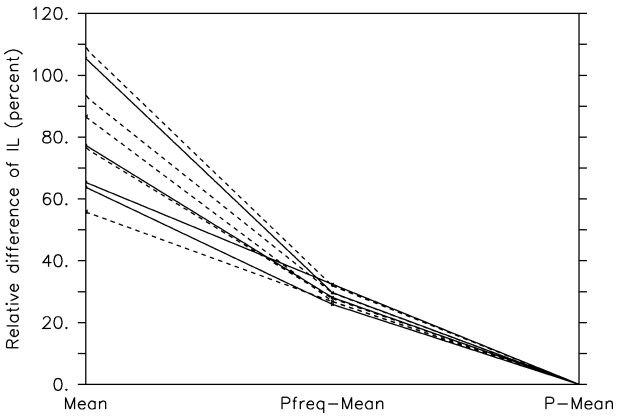

FIG. 11. Evolution of the relative difference of interception loss with the progressive disaggregation of precipitation; the reference is simulation P-mean [solid (dashed) lines correspond to humid (dry) grid boxes].

generating mechanism. A model with an infiltration-excess mechanism of runoff production is more sensitive to the precipitation spatial variability than a model with a saturation-excess mechanism like ours (Giorgi 1997; Koren et al. 1999). There may also be a compensating effect between the changes in the surface runoff and in the subsurface runoff (or drainage).

5. Disaggregation of the atmospheric forcings

The objective of this section is to understand the relative importance of the different forcings in the simulation of the water balance by ORCHIDEE and primarily to emphasize the strong effect of the precipitation subgrid-scale variability. For this purpose, the second group of simulations will be used (cf. Table 2).

Several authors point out that precipitation subgrid-scale variability has a first-order effect on the exchanges between the surface–biosphere and the atmosphere (Pitman et al. 1990; Dolman and Gregory 1992; Pitman et al. 1993; Seth et al. 1994; Ghan et al. 1997; Wang and Eltahir 2000). Spatial heterogeneities of the vegetation cover also have a significant and combined effect (Seth et al. 1994). The effect of the vegetation cover will not be studied here even if the vegetation cover might influence the partitioning of precipitation between evapotranspiration and runoff and also the soil water content.

a. Dominant influence on precipitation

Figure 14 compares the local annual runoff of simulations mean and P-mean to simulation Agg20. The correlation coefficient goes from 0.31 for simulation mean to 0.98 for simulation P-mean. This large increase underlines the important influence of the precipitation subgrid-scale variability on the runoff simulation. This point is confirmed by Fig. 15, which compares the regional runoff and interception loss amounts in various simulations of the second group to simulation Agg20. At least 75% of the runoff of simulation Agg20 is reproduced in simulation P-mean and the interception loss increase is reduced by 20%–80% of the reference interception loss.

This study is thus consistent with others: precipitation spatial and temporal distributions have a first-order effect on the water cycle simulation. Yet, there is still a significant difference between the values of simulations P-mean and Agg20.

b. The other forcing variables

The mismatch of the results between simulations P-mean and Agg20 can be attributed to other atmospheric forcings besides precipitation. Figure 15 suggests that radiation and wind subgrid-scale variabilities have little impact on the regional annual water balance, whereas when the three thermodynamic variables, air temperature, humidity, and surface pressure are disaggregated all together, the regional annual results are modified significantly and get very close to the results obtained in Agg20. This difference between the forcings influences remains true at smaller time scales. As an example, Fig. 16 compares the temporal evolutions of interception loss for each simulation of the second group in the humid region (region B).

Solar radiation corresponds to the energy input in the system. The very small influence of its subgrid-scale variability on the results is quite suprising. It may be explained by the fact that long- and shortwave radiation vary essentially slowly with latitude (the spatial variation along the latitude is already partly taken into account at the coarsest resolution). Solar radiation at the surface depends largely on the cloud coverage, which

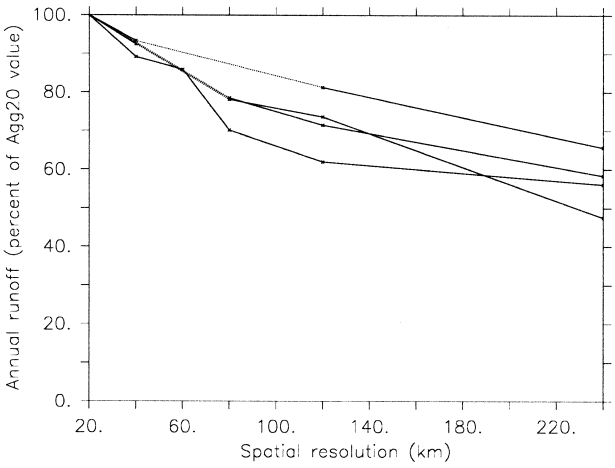

(a) Annual runoff (percent of Agg20)

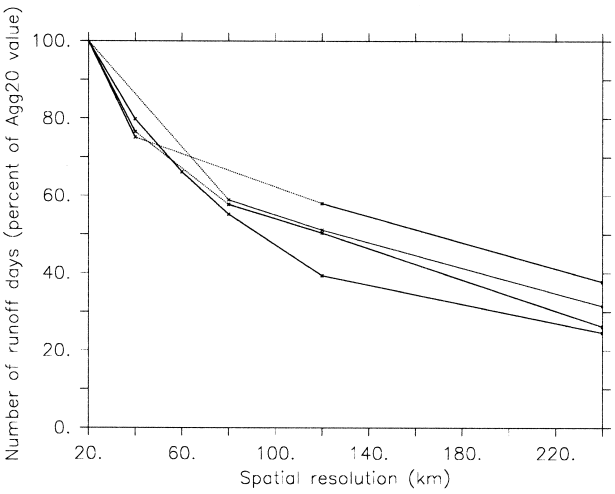

(b) Number of runoff days (percent of Agg20)

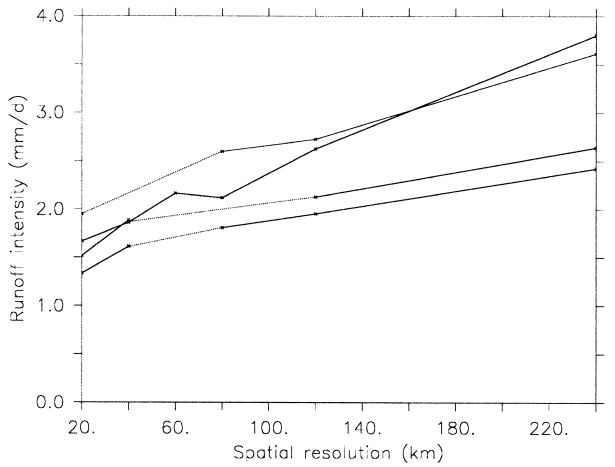

(c) Runoff intensity (mm/day of runoff)

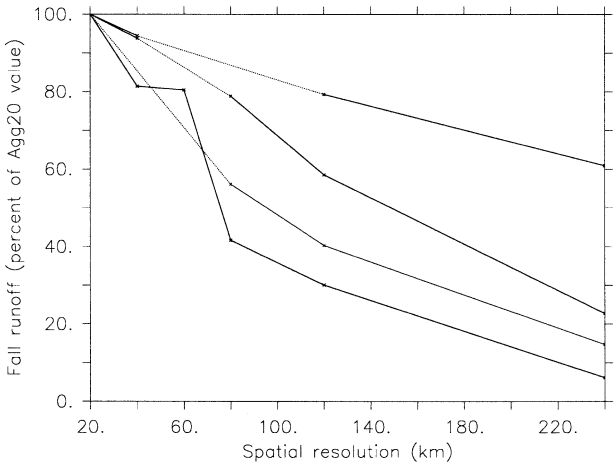

(a) Fall runoff (percent of Agg20)

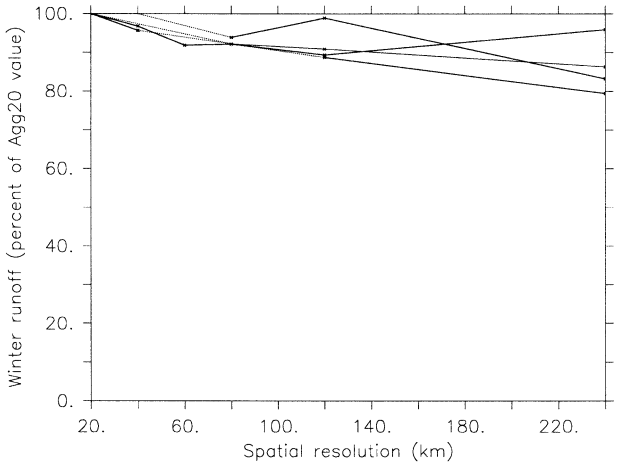

(b) Winter runoff (percent of Agg20)

FIG. 13. Seasonal effects of the aggregation of the forcings on the runoff generation in the Agg simulations (the reference is simulation Agg20): (a) fall runoff (% of Agg20) and (b) winter runoff (% of Agg20).

may be quite homogeneous over a region when averaged over a time step.

In the model, the wind influences the latent heat flux through the aerodynamic resistance, which is inversely proportional to the wind speed. Its subgrid-scale variability seems to have little impact on the water balance. In fact, disaggregating the wind slightly increases the maximum values (not shown).

On the contrary, the three thermodynamic variables seem to play an important role (cf. Fig. 16b). One of

←

FIG. 12. (a) Mean annual runoff (% of Agg20), (b) number of runoff days (% of Agg20), and (c) runoff intensity (mm day^{-1} of runoff) vs spatial resolution (for simulations Agg20–Agg240) at 240-km resolution.

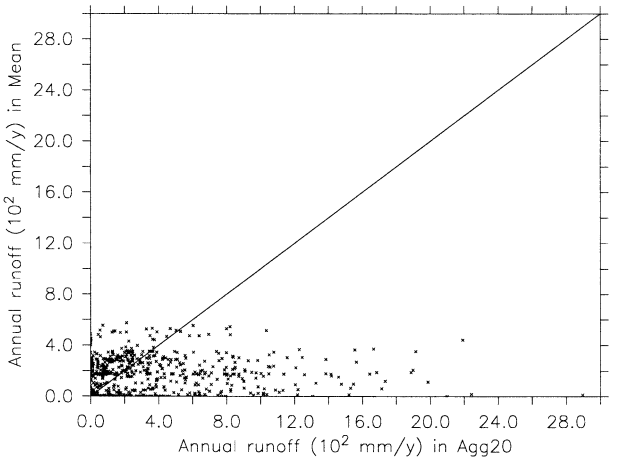

(a) Mean/Agg20

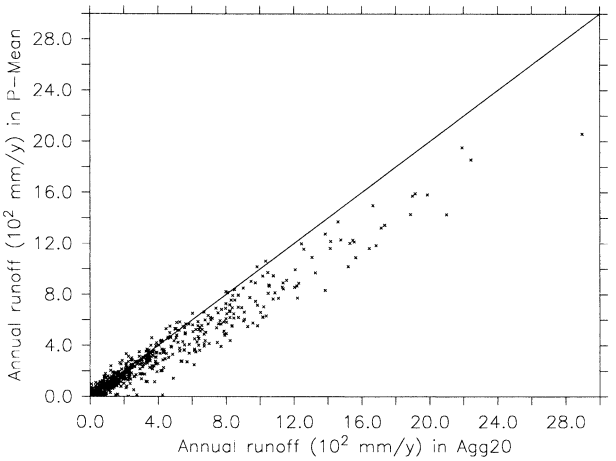

(b) P-Mean/Agg20

FIG. 14. Annual values of runoff (10^2 mm yr^{-1}) in simulations (a) mean and (b) P-mean vs annual values of runoff in simulation Agg20 (10^2 mm yr^{-1}).

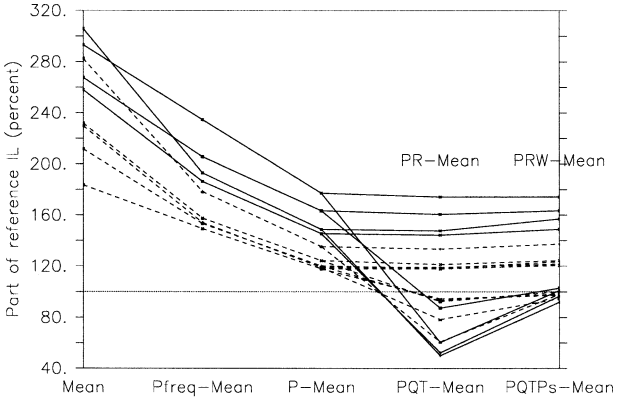

(a) Interception loss

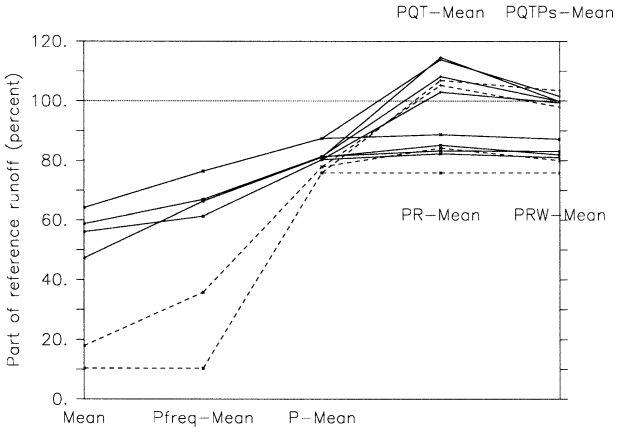

(b) Runoff

FIG. 15. Evolution of the mean annual large-scale (a) interception loss and (b) runoff with the choice of the disaggregated forcings [solid (dashed) lines correspond to humid (dry) grid boxes].

the main differences between Agg20 and P-mean is the occurrence of negative interception loss values, that is, dew. These negative values that occur principally during the cold season have disappeared in P-mean but they are present in simulation PTQPs-mean, which is consequently very close to Agg20.

In ORCHIDEE, the latent heat flux is proportional to the difference of the specific humidity at air saturation at the soil temperature and the air humidity at the same time. When this difference becomes negative, water is deposited on the vegetation without limitation and transpiration is blocked completely. This corresponds to dew. Dew happens in the model mainly in winter, when the temperature happens to increase rapidly. Soil temperature adapts itself to the change but with a small delay, thus making the occurrence of dew possible. When the thermodynamic forcings are averaged, temperature contrasts are reduced and so is dew occurrence. When only air humidity and temperature are disaggregated and surface pressure remains averaged (simulation PTQ-mean), the process of dew is reinforced and largely overestimated, which explains the much smaller and even negative values of spatially averaged interception loss in winter in that case (cf. Fig. 16). Localized low surface pressures correspond to cold temperatures where the dew process tends to happen. In this case, the air specific humidity at the soil temperature is reduced by an increased surface pressure, and the occurrence of negative values is thus increased. The effect of overestimating dew is still strong when only air humidity is disaggregated (not shown). The influence of dew is made important by the fact that, when it occurs, transpiration is blocked and there is no limiting factor to the negative latent heat flux. However, in this experiment, there may be a need for feedbacks to the atmosphere when dew deposition is occurring.

The aim of this section has been to study the importance of the subgrid-scale variability of the different

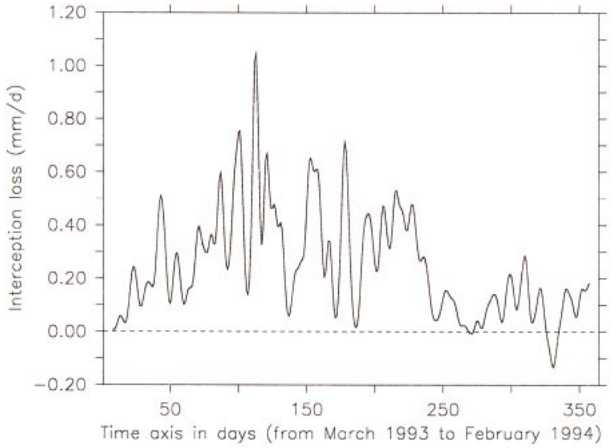

(a) Interception loss in Agg20

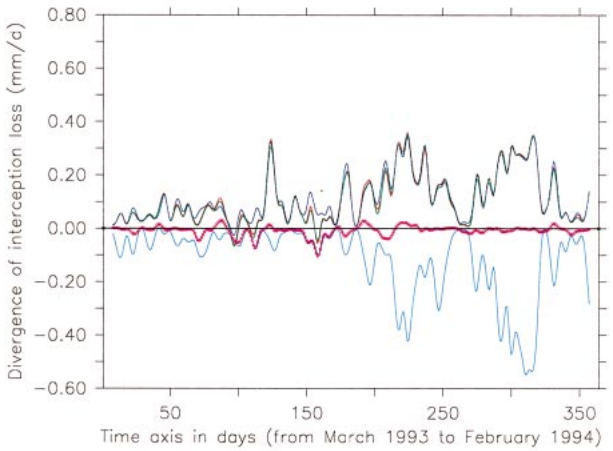

(b) Difference with Agg20

FIG. 16. (a) Interception loss (mm day^{-1}) in the humid region for simulation Agg20; (b) for the same region but for difference of interception loss between Agg20 and different simulations (P-mean, red; PR-mean, green; PRW-mean, blue; PTQ-mean, light blue; PTQPs-mean, purple); a binomial window of 15 days was applied to smooth each variable along the temporal axis.

forcing variables. We first emphasized that precipitation has a dominant effect on the water balance simulation in this region. The main features of the hydrological cycle are recontructed in simulation P-mean. But the interception loss still remains overestimated. The results are, as a second-order effect, influenced by three thermodynamic variables (temperature, air humidity, and surface pressure), which must have the same spatial resolution to correctly estimate dew.

6. Summary and conclusions

In the broad context of the regional impacts of a climatic change, our study has focused on the dependence of simulated hydrological processes to the spatial resolution of the forcings. The land surface model ORCHIDEE has been used with prescribed radiative and atmospheric forcings. These prescribed forcings are the outputs of the regional climate model PROMES over the Iberian Peninsula. Its spatial resolution (20 km × 20 km) is much higher than the resolution of a typical general circulation model. In the first experiment, the PROMES outputs have been aggregated stepwise to the typical resolution of a GCM (240 km × 240 km), and applied to ORCHIDEE, in order to analyze the impacts of the changing resolution on the simulated water balance. Then, subgrid-scale variability for the different forcings and for the land surface has been progressively reintroduced. This second experiment aimed at isolating the crucial elements of subgrid-scale variability.

The results presented here must be considered within the limits of the experimental design. The forcings are the outputs of a model over a limited area for only one year. Even if the selected year is supposed to be representative of the Iberian climate, these results do not take into account interannual variability. The simulations are performed in a stand-alone mode, consequently preventing any feedback from the land surface to the atmosphere. Only the model ORCHIDEE was used in this experiment.

The main consequences of the progressive aggregation of the forcings, particularly of precipitation, have been studies first. The primary effect of the aggregation on the water cycle is the significant increase of interception loss. This increase may lead to unrealistic values of the interception ratio, particularly over dry regions, when the spatial resolution is coarser than 100 km. Our study points out that this interception loss increase depends principally on the precipitation frequency (whether it rains or not locally) and less on the precipitation intensity. It is noted that precipitation frequency is directly related to the regional precipitation coverage (what fraction of the region is reached by the rain).

The next effect of the aggregation on the forcings is the decrease of runoff production in the northern humid region. This decrease is explained by the reduction of runoff frequency and can reach 55% of the high-resolution runoff value. This occurs mainly during the period when the soil reservoir is filling, in fall and early winter.

These induced impacts of the aggregation on the foliage interception and on runoff occurrence drive the adjustment of the other hydrological components, depending on the climate. The redistribution of precipitation between runoff, transpiration, interception loss, and bare soil evaporation is modified when the forcings are aggregated. In the dry region, the increase of interception loss is compensated by a reduced transpiration and the soil water content is reduced. This underlines the importance of the resolution in GCMs for the simulation of soil moisture content. In the humid region, runoff is delayed and ends earlier due to the increased interception loss and the reduced spatial variance of the water input.

Then, with the second experiment, the influence of the different input variables has been studied. First, it must be noted that precipitation has a dominant effect on the regional water balance and on the local hydrological processes. When the only disaggregated forcing is precipitation, the main features of the hydrological cycle are reconstructed. Two major points can be underlined then: 1) solar radiation and wind have little influence on the results whereas air temperature and humidity, and surface pressure, have significant impact on the results; 2) the three last variables must have the same spatial resolution; otherwise, the dew estimation is erroneous and the water balance perturbed.

This study has concentrated on the dependence of simulated hydrological processes on the spatial resolution of the forcings. Both major types of heterogeneities, the heterogeneity of the land surface and the subgrid-scale variability of the climatic variables, are noted to be of significant importance. It also seems to be crucial that there is consistency between the scales of the different components of the climatic system. The introduction of subgrid-scale variability in the land surface models has been largely studied (topography, distribution of vegetation, hydrological processes like runoff) and is implemented in many land surface models (Boone et al. 2003). Atmospheric forcings with the same spatial level of detail may be needed to prevent scale mismatches between land surface processes and large-scale atmospheric circulation.

The resolution of the PROMES outputs, 20 km $\times$ 20 km, is considered to be the ''the truth'' in our experiments. However, there is still a large subgrid-scale variability in the hydrological processes at this resolution. How would the results be modified with higher spatial resolution forcings? It seems that the dependence of the water balance on the spatial scale of the forcings depends on this scale and is weaker at resolutions higher than those like the PROMES resolution. This has been noted for the variable runoff in a recent study (Koren et al. 1999) involving three hydrological models with very high resolution precipitation data (4 km $\times$ 4 km). The evolution of the water balance with resolution would become significant only beyond a certain threshold. This threshold might be related to the size of the weather systems over the considered region.

Acknowledgments. The authors thank the Facultad de Ciencias del Medio Ambiente (Spain) for providing the simulation of the regional climate model PROMES. They also thank Patricia De Rosnay and Bryant McAvaney for their helpful comments and early review of the paper. The simulations used in this study were performed using the computational facilities of the Institut du Développement et des Ressources en Informatique Scientifique (CNRS, France). We would also like to thank the three referees for their comments, which have greatly helped us to improve the manuscript.

APPENDIX A

The Vegetation Distribution in ORCHIDEE

The IGBP 1-km global land cover map (Belward et al. 1999) reduced by a dominant-type method to 5 km $\times$ 5 km spatial resolution is used with the Olson classification (96 types) (Olson et al. 1983). This map prescribes the fraction of each vegetation type over each 5 km $\times$ 5 km cell. To simplify the cover description, the data are reduced to percentages of 13 more basic plant functional types (PFTs): bare soil, tropical broad-leaved evergreen and raingreen trees, temperate needle- and broad-leaved evergreen and summergreen trees, boreal needle- and broad-leaved evergreen trees summergreen, C3 and C4 grasslands, and C3 and C4 cultures. The C3 plants make a three-carbon compound as the first stable product of carbon fixation whereas C4 plants make a four-carbon cycle during initial carbon fixation, which eventually increases the efficient net photosynthesis. The C4 plants, like maize or sugar cane, represent less than 1% of the plants.

These 13 PFTs can simultaneously share the same grid box. Each of them occupies a specified fraction of the grid box, calculated using the modified Olson percentages within the grid box. The calculation can be made for any spatial resolution above 5 km $\times$ 5 km. For each vegetation class, latent heat flux is computed independently. A mean flux for the grid box is then computed from a weighted average of these fluxes.

APPENDIX B

The Routing Scheme

The routing scheme in this paper uses a map of the world basins built by combining the map built at the University of New Hampshire by Vörösmarty et al. (2000) and the one built by Oki et al. for the Total Runoff Integrating Pathways (TRIP) scheme (Oki et al. 1999). At each time step, the runoff and ''drainage'' fluxes are temporarily stored in three reservoirs, which have different residence time constants. The water is progressively routed to the oceans, following the main slopes and taking into account the tortuosity of the river channels, through a cascade of linear reservoirs. ''Drainage'' flux is taken as part of the calculated saturation-excess runoff. This fraction is constant and chosen in an arbitrarian way.

APPENDIX C

Brief Presentation of the Soil–Plant System

In ORCHIDEE, for each vegetation type, the transpiration (Tr) and interception loss (IL) fluxes are computed using the following expressions:

$$\mathrm{Tr} = \left(1 - \frac{I}{I_{\max}}\right) U_s \rho \frac{\delta q}{r_a + r_o + r_c} \quad \text{and}$$

$$\mathrm{IL} = \frac{I}{I_{\max}} \rho \frac{\delta q}{r_a + r_o},$$

where I is the amount of water stored on the foliage ($I_{\max}$ is its maximum value), U_s is the ability of roots to extract water for a given soil moisture, and ρ is the air density. Transpiration and interception loss are driven by δq, the gradient of specific humidity between the evaporating surface and the overlying air, and limited by a sum of resistances r_a, r_o, and r_c, which accounts for vegetation and aerodynamic effects.

More precisely, the aerodynamic resistance, r_a, is inversely proportional to the product of the drag coefficient and the wind speed. The architectural resistance, r_o, represents the aerodynamic conductance between the leaves and the top of the canopy. The canopy or bulk stomatal resistance, r_c, depends on the net solar radiation and the water vapor deficit of the air above the canopy and is inversely proportional to the leaf area index (LAI). The maximum amount of water stored on the foliage, $I_{\max}$, is defined for each vegetation type and it depends only on the LAI. It does not depend on the precipitation properties (intensity), which could be a significant dependence (Ramírez and Senarath 2000). Here, U_s is a water uptake function that depends on vegetation type through a parameter of the root profile and on soil water depletion. This function represents the ability of roots to extract water from the soil (de Rosnay and Polcher 1998).

The bare soil evaporation is expressed by

$$E\mathrm{soil} = U_s \rho \frac{\delta q}{r_a + r_{\mathrm{soil}}},$$

where r_{soil} is the soil resistance and is defined as $r_{\mathrm{soil}} = h_s r_t$ ($r_t = 33\,000$ s m^{-2} is the resistance by meter of dry soil and h_s the dry soil height). The high level of this resistance implies that a dry soil height of 1 cm creates a soil resistance of $r_{\mathrm{soil}} = 330$ s m^{-1}, which largely limits bare soil evaporation.

Consequently, soil moisture controls transpiration through a vegetation-dependent function representing the ability of roots to extract water, U_s, and bare soil evaporation through a soil resistance, r_{soil}, which depends on the dry soil height at the surface.

The behavior of the two moisture layers and the control of evaporation by the soil–plant system are described more fully by de Rosnay and Polcher (1998).

REFERENCES

Arola, A., and D. Lettenmaier, 1996: Effect of subgrid spatial heterogeneity on GCM-scale land surface energy and moisture fluxes. *J. Climate,* **9,** 1339–1349.

Arribas, A., C. Gallardo, M. Gaertner, and M. Castro, 2003: Sensitivity of the Iberian Peninsula climate to a land degradation. *Climate Dyn.,* **20,** 477–489.

Belward, A., J. Estes, and K. Kline, 1999: The IGBP-DIS Global 1-km Land-Cover Data Set DISCover: A project overview. *Photogramm. Eng. Remote Sens.,* **9,** 1013–1020.

Bolle, H.-J., Ed., 2003: *Mediterranean Climate, Variability and Trends.* Springer, 320 pp.

Boone, A., and Coauthors, 2004: The Rhône-Aggregation land surface scheme intercomparison project: An overview. *J. Climate,* **17,** 187–208.

Calder, I., 1990: *Evaporation in the Uplands.* John Wiley and Sons, 148 pp.

de Rosnay, P., and J. Polcher, 1998: Modelling root water uptake in a complex land scheme coupled to a GCM. *Hydrol Earth Syst. Sci.,* **2,** 239–255.

Dolman, A., and D. Gregory, 1992: The parameterization of rainfall interception in GCMs. *Quart. J. Roy. Meteor. Soc.,* **118,** 455–467.

Ducharne, A., K. Laval, and J. Polcher, 1998: Sensitivity of the hydrological cycle to the parameterization of soil hydrology in a GCM. *Climate Dyn.,* **14,** 307–327.

Ducoudré, N., K. Laval, and A. Perrier, 1993: A new set of parameterizations of the hydrologic exchanges and the land–atmosphere interface within the LMD atmospheric global circulation model. *J. Climate,* **6,** 248–273.

Entekhabi, D., and P. Eagleson, 1989: Land surface hydrology parameterization for atmospheric general circulation models including subgrid-scale spatial variability. *J. Climate,* **2,** 816–831.

Gaertner, M., O. Christensen, J. Prego, J. Polcher, C. Gallardo, and M. Castro, 2001: The impact of deforestation on the hydrological cycle in the western Mediterranean: An ensemble study with two regional climate models. *Climate Dyn.,* **17,** 857–873.

Gash, J., C. Lloyd, and G. Lachaud, 1995: Estimating sparse forest rainfall interception with an analytical model. *J. Hydrol.,* **170,** 79–86.

Ghan, S., J. Liljegren, W. Shaw, J. Hubbe, and J. Doran, 1997: Influence of subgrid variability on surface hydrology. *J. Climate,* **10,** 3157–3166.

Giorgi, F., 1990: Simulation of regional climate using a limited area model nested in a general circulation model. *J. Climate,* **3,** 941–963.

——, 1997: An approach for the representation of surface heterogeneity in land surface models. Part II: Validation and sensitivity experiments. *Mon. Wea. Rev.,* **125,** 1900–1919.

——, and L. Mearns, 1991: Approaches to the simulation of regional climate change: A review. *Rev. Geophys.,* **29,** 191–216.

——, and ——, 1999: Introduction to special selection: Regional climate modeling revisited. *J. Geophys. Res.,* **104,** 6335–6352.

Haddeland, I., B. Matheussen, and D. Lettenmaier, 2002: Influence of spatial resolution on simulated streamflow in a macroscale hydrologic model. *Water Resour. Res.,* **38**, 1124, doi:10.1029/2001WR000854.

Hewitson, B., and R. Crane, 1996: Climate downscaling: Techniques and application. *Climate Res.,* **7,** 85–95.

Koren, V., B. Finnerty, J. Schaake, M. Smith, D.-J. Seo, and Q.-Y. Duan, 1999: Scale dependencies of hydrologic models to spatial variability of precipitation. *J. Hydrol.,* **217,** 285–302.

Koster, R., M. Suarez, A. Ducharne, M. Stieglitz, and P. Kumar, 2000: A catchment-based approach to modeling land surface processes in a general circulation model. 1-model structure. *J. Geophys. Res.,* **105,** 24 809–24 822.

Liang, X., and Z. Xie, 2001: A new surface runoff parameterization with subgrid-scale heterogeneity for land surface models. *Adv. Water Resour.,* **24,** 1173–1193.

——, D. P. Lettenmaier, and E. F. Wood, 1996: One-dimensional statistical dynamic representation of subgrid spatial variability of precipitation in the two-layer variable infiltration capacity model. *J. Geophys. Res.,* **101,** 21 403–21 422.

Lloyd, C., and A. Marques, 1988: Spatial variability of throughfall measurements in Amazonian rainforest. *Agric. For. Meteor.,* **43,** 277–294.

Loustau, D., P. Berbigier, and A. Granier, 1992: Interception loss,

throughfall and stemflow in a maritime pine stand. II. An application of Gash's analytical model of interception. *J. Hydrol.*, **138,** 469–485.

Mearns, L., I. Bogardi, F. Giorgi, I. Matyasovszky, and M. Palecki, 1999: Comparison of climate change scenarios generated from regional climate model experiments and statistical downscaling. *J. Geophys. Res.*, **104,** 6603–6621.

Milly, P., and P. Eagleson, 1988: Effects of storm scale on surface runoff volume. *Water Resour. Res.,* **24,** 620–624.

New, M., M. Hulme, and P. Jones, 2000: Representing twentieth-century space–time climate variability. Part II: Development of 1901–96 monthly grids of terrestrial surface climate. *J. Climate,* **13,** 2217–2238.

Oki, T., T. Nishimura, and P. Dirmeyer, 1999: Assessment of annual runoff from land surface models using total runoff integrating pathways (TRIP). *J. Meteor. Soc. Japan,* **77,** 235–255.

Olson, J., J. Watts, and L. Allison, 1983: Carbon in live vegetation of major world ecosystems. Tech. Rep. W-7405-ENG-26, Oak Ridge National Laboratory, Oak Ridge, TN, 152 pp.

Pitman, A., A. Henderson-Sellers, and Z.-L. Yang, 1990: Sensitivity of regional climates to localized precipitation in global models. *Nature,* **346,** 734–737.

——, Z.-L. Yang, and A. Henderson-Sellers, 1993: Subgrid-scale precipitation in AGCMs: Reassessing the land surface sensitivity using a single column model. *J. Climate,* **9,** 33–41.

Ramírez, J., and S. U. Senarath, 2000: A statistical–dynamical parameterization of interception and land surface–atmosphere interactions. *J. Climate,* **13,** 4050–4063.

Rutter, A., 1975: The hydrological cycle in vegetation. *Vegetation and the Atmosphere,* J. L. Monteith, Ed., Vol. 1, Academic Press, 111–154.

Scurlock, J., G. Asner, and S. Gower, 2001: Worldwide historical estimates and bibliography of leaf area index, 1932–2000. ORNL Tech. Memo. TM-2001/268, Oak Ridge National Laboratory, Oak Ridge, TN, 23 pp.

Seth, A., F. Giorgi, and R. Dickinson, 1994: Simulating fluxes from heterogeneous land surfaces: Explicit subgrid method employing the Biosphere–Atmosphere Transfer Scheme (BATS). *J. Geophys. Res.,* **99,** 18 651–18 667.

Sitch, S., and Coauthors, 2000: LPJ—A coupled model of vegetation dynamics and the terrestrial carbon cycle. The Role of Vegetation Dynamics in the Control of Atmospheric CO_2 Content, Ph.D. thesis, Lund University.

Tank, A., and Coauthors, 2002: Daily dataset of 20th-century surface air temperature and precipitation series for the European Climate Assessment. *Int. J. Climatol.,* **22,** 1441–1453.

Ubarana, V., 1996: Observation and modeling of rainfall interception loss in two experimental sites in Amazonian forest. *Amazonian Deforestation and Climate,* J. H. C. Gash et al., Eds., John Wiley and Sons, 151–162.

van Dijk, A., and L. Bruijnzeel, 2001: Modelling rainfall interception by vegetation of variable density using an adapted analytical model. Part 2. Model validation for a tropical upland mixed cropping system. *J. Hydrol.,* **247,** 239–262.

Viovy, N., 1996: Interannuality and CO2 sensitivity of the SECHIBA-BG coupled SVAT–BGC model. *Phys. Chem. Earth,* **21,** 489–497.

Vörösmarty, C., B. Fekete, B. Meybeck, and R. Lammers, 2000: Global system of rivers: Its role in organizing continental land mass and defining land-to-ocean linkages. *Global Biogeochem. Cycles,* **14,** 599–621.

Wang, G., and E. Eltahir, 2000: Modeling the biosphere–atmosphere system: The impact of the subgrid variability in rainfall interception. *J. Climate,* **13,** 2887–2899.

Warrach, K., M. Stieglitz, H.-T. Mengelkamp, and E. Raschke, 2002: Advantages of a topographically controlled runoff simulation in a soil–vegetation–atmosphere transfer model. *J. Hydrometeor.,* **3,** 131–148.

Waterloo, M., L. Bruijnzeel, and H. Vugts, 1999: Evaporation from *Pinus caribaea* plantations on former grassland soils under maritime tropical conditions. *Water Resour. Res.,* **35,** 2133–2144.

Wood, E., D. Lettenmaier, and V. Zartarian, 1992: A land-surface hydrology parameterization with subgrid variability for general circulation models. *J. Geophys. Res.,* **97,** 2717–2728.

Zorita, E., and H. von Storch, 1999: The analog method as a simple statistical downscaling technique: Comparison with more complicated methods. *J. Climate,* **12,** 2474–2489.